Silicate and sulphide mineralogy, and conditions of equilibration of ultramafic rocks of the Indo-Myanmar ophiolite belt between Tusom, Manipur and Shomra village, Myanmar

Nirupama Khwairakpam, Maibam Bidyananda* and Sanjenbam Shyamson Singh

Department of Earth Sciences, Manipur University, Canchipur, Imphal 795 003, India

The northeast-India ophiolite complex is exposed in many parts of Nagaland and Manipur, with particularly well-preserved mantle-sequence peridotite present in its southern section in Manipur state. We present the results of an investigation into the petrology and constituent mineral chemistry of this peridotite, which is associated with the Indo-Myanmar ophiolite located between Tusom, Ukhrul District (Manipur) and Shomra village (Myanmar). Mineral compositions indicate that it is an abyssal peridotite that has undergone minimal partial melting (1–5%). Equilibration probably occurred in the upper mantle at a temperature of 1080–1240°C, a pressure of 23–24 kbar, and an oxygen fugacity between 0.303 and 0.580 log units above the FMQ buffer. Primary and secondary sulphide phases in the studied peridotites have also been analysed. Pentlandite ((Fe,Ni)$_9$S$_8$) was found to be the primary sulphide mineral, which occurred in association with orthopyroxene and awaruite (Ni$_3$Fe). Cu-rich alloys and magnetite occur as secondary minerals that developed during later serpentinization.

Keywords: Abyssal peridotite, equilibrium temperature, pentlandite, metal alloys, oxygen fugacity, partial melting.

THE compositions of phases in ophiolitic, mantle-derived ultramafic rocks depend upon the degree and pressure–temperature conditions of partial melting, and the effects of magma–rock interaction[1]. Mineral compositions in mantle peridotites are considered to be reliable petrogenetic indicators. Although a few studies of the ophiolitic mantle section of Ukhrul district (Manipur side) are available[2–4], studies of its continuation onto the Myanmar side are lacking. In this study, we analysed primary silicate mineral phases within mantle rocks exposed between Tusom village, Manipur, and Shomra village, Myanmar, to elucidate their equilibrium conditions of formation and related intensive parameters. We also analysed metal sulphides and metallic alloys in the ultramafic rock and present an interpretation of the probable formation of these phases.

The Indo-Myanmar Ophiolite belt, approximately 200 km long, extends from Nagaland in the north to Manipur in the south. It is a NNE–SSW trending, westerly convex linear belt and is mostly restricted to the eastern section of Indo-Myanmar Range. The belt has an average width of ~15 km in its northern sector (Nagaland) but gradually narrows to a width of a few metres at its southern end (Manipur). The ophiolite belt consists of lensoid bodies interbedded with Disang flyschoids, which are highly tectonized and dismembered. Despite having undergone varying degrees of serpentinization, relict primary minerals are preserved in some rocks. A traverse map showing the study area is shown in Figure 1. Major-element compositions of mineral phases were determined by electron probe microanalysis (EPMA) using a Jeol JXA 8900 RL in wavelength dispersive mode. Silicate phases were analysed using an accelerating potential of 20 kV, a beam current of 12 nA, and a spot size of 2 µm. Natural minerals and oxides (for Si, Ti, Al, Fe, Mg, Mn, Cr and Zn), and pure metal (for V, Co) were used as standards. The mineralogy of Fe–Ni–Cu sulphides – as well as their textural relationships with silicates and Cr-spinel – was studied in detail via examination of polished thin sections at various magnifications (100- and 500-times) using an optical microscope. Cu, Co, and Ni contents were analysed by comparison with pure metal standards, whereas S and Fe contents were analysed against a natural pyrite. Operating conditions for EPMA were 15 nA beam current, 20 kV accelerating voltage, 10 s counting times (10 s/peak, 10 s/background) for Ni and S, and 60 s counting times (60 s/peak; 60 s background) for Fe, Cu, and Co.

The samples studied are orthopyroxene-dominated peridotite (i.e. harzburgite), and we focused on units that contained relict primary minerals and sulphide mineralization. The proportion of secondary serpentine-mineral
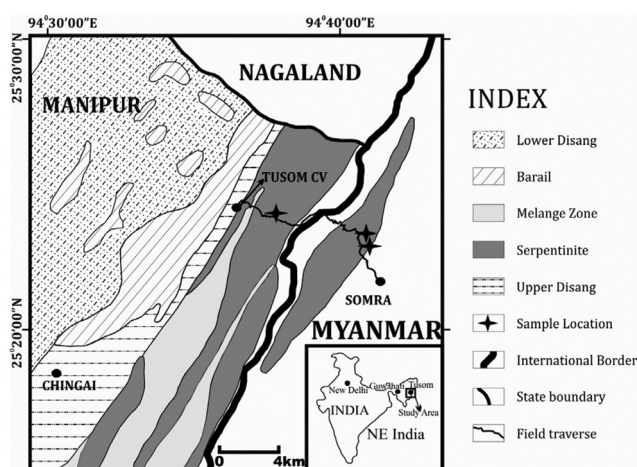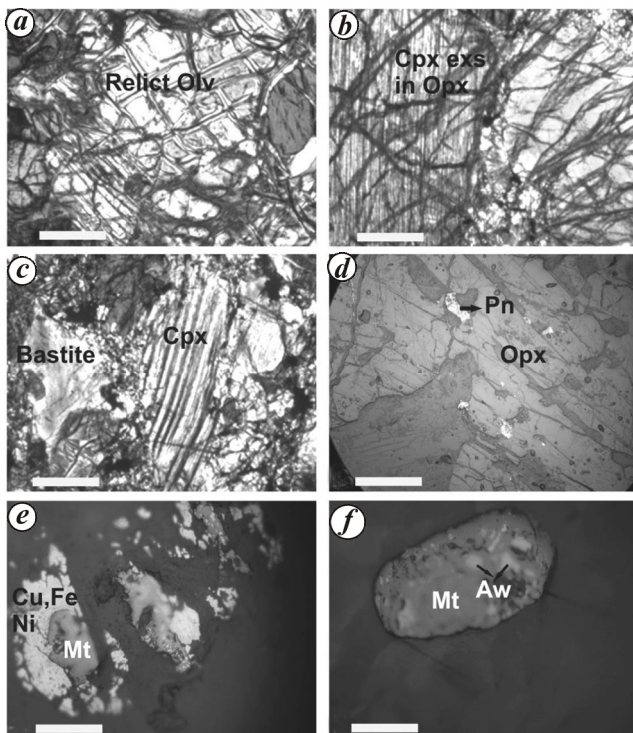

Figure 1. Traverse map of the study area.

alteration in different protoliths ranged between 49% and 78%. The majority of the studied samples exhibited aphaneritic texture. Phenocrysts of orthopyroxene, clinopyroxene and – less frequently – olivine were surrounded by finer grains, which were mostly altered.

Olivine was typically medium-grained and highly fractured, and was commonly found to have been altered to serpentine. Unaltered, relic olivine was present in the matrix of fibrous serpentine in some of the studied samples (Figure 2 a). After olivine, orthopyroxene was the next most abundant mineral, comprising 12–24% volume, and occurring mostly as coarse anhedral to subhedral grains. It frequently exhibited fine exsolution lamellae of clinopyroxene (Figure 2 b). Grains with curved cleavages and undulatory extinction were interpreted to record clear evidence of post-crystallization tectonic disturbance (Figure 2 c).

Alteration of orthopyroxene to bastite (a serpentine pseudomorph after pyroxene) was often observed. Bastite showed undulatory extinction, with a bronze/metallic lustre or schiller, and comprised 2–4% volume of the studied samples. Clinopyroxene was medium grained, anhedral to subhedral in shape, and comprised 3–8% volume. Spinel occurred as unaltered anhedral or amoeboidal

crystals between grain boundaries of other minerals and comprised 1–7% volume.

Representative compositional data for all silicate minerals are given in Table 1. Olivine exhibited forsterite contents of $Fo_{89.7–90.3}$. MnO varied from 0.11 to 0.21 wt%, and the CaO content was low (<0.04 wt%). NiO content showed only a minor variation (0.32–0.43 wt%). The olivine grains studied lie on the mantle array on both the NiO versus Fo and MnO versus Fo content plots (Figure 3).
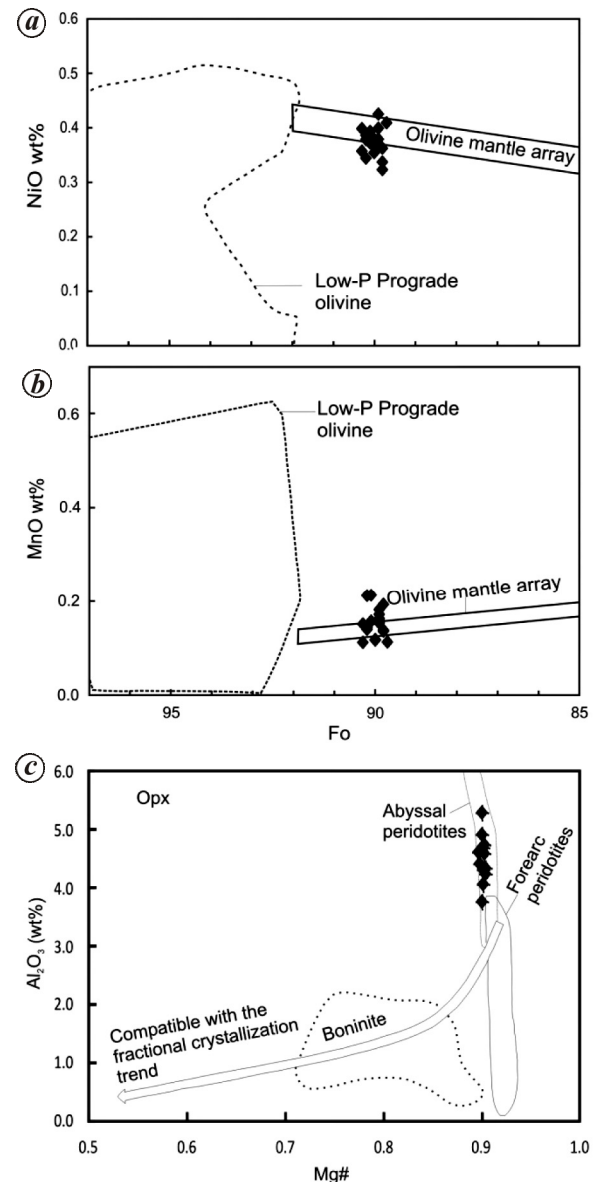
Figure 3. a, b, Forsterite (Fo) against NiO and MnO (wt%) contents for olivine of the studied Shomra peridotites. Field for olivine mantle array is after Takahashi et al.[17] and the low pressure prograde olivine field after Khedr and Arai[18]. Note that olivine lies in the extended trend of the olivine mantle array, possibly showing features of mantle residual olivine. c, Variation diagrams of Al_2O_3 versus Mg# for the studied orthopyroxene. The fields of abyssal peridotite and forearc peridotite are from Johnson et al.[8], Ishii et al.[19] and boninite from Seo et al.[20]. The arrow, compatible with the fractional crystallization trend is from Constantin[21].

Figure 2. a, Orthopyroxene showing exsolved clinopyroxene in peridotite. Field of view (FOV) is 23 mm. b, Clinopyroxene porphyroclast coexisting with bastite. Note the banded lamellae in the clinopyroxene. FOV – 23 mm. c, Relict clinopyroxene in serpentinized peridotite. FOV – 23 mm. d, Olivine showing mesh fractures. FOV – 23 mm. e, Amoeboidal spinels in serpentinites. FOV – 35 mm. f, Bastite coexisting with spinels in serpentinized peridotite. FOV – 35 mm.

Table 1. Representative mineral compositions of the studied samples

Mineral	Olivine						Orthopyroxene					Clinopyroxene					Spinel			
Sample no.	2b-9	2b-9	6a-9	6a-9	1d-8	1d-8	2b-9	2b-9	6a-9	1d-8	1d-8	2b-9	2b-9	6a-9	1d-8	1d-8	2b-9	2b-9	1d-8	1d-8
Spot no.	4	9	19	21	34	53	6	14	25	42	48	16-n	20-n	22	23	1-n	17-n	12	7-n	8-n
SiO_2	41.01	40.84	40.19	40.39	40.08	40.30	56.20	55.37	54.70	54.79	55.00	52.27	52.23	51.58	51.64	52.03	0.02	0.01	0.04	0.00
Al_2O_3	0.00	0.00	0.00	0.00	0.00	0.02	4.05	4.32	5.29	4.74	4.59	4.88	4.51	7.35	6.96	5.92	53.74	46.79	56.61	56.62
Na_2O	0.00	0.00	0.01	0.00	0.01	0.00	0.02	0.00	0.07	0.08	0.02	1.18	0.82	1.97	1.83	0.97	0.00	0.00	0.07	0.08
K_2O	0.00	0.00	0.00	0.00	0.00	0.00	0.01	0.00	0.00	0.01	0.01	0.00	0.00	0.00	0.00	0.01	0.00	0.00	0.00	0.01
MnO	0.18	0.21	0.15	0.19	0.14	0.16	0.16	0.15	0.18	0.18	0.17	0.09	0.08	0.09	0.08	0.11	0.14	0.11	0.11	0.13
CoO	0.04	0.04	0.05	0.02	0.02	0.03	0.03	0.00	0.03	0.02	0.02	0.03	0.02	0.04	0.03	0.02	0.09	0.09	0.06	0.05
MgO	48.62	48.88	49.27	49.19	49.52	49.24	32.30	32.40	32.14	32.42	32.73	15.24	15.86	13.91	14.56	16.71	19.59	16.36	19.80	19.97
TiO_2	0.01	0.00	0.02	0.02	0.00	0.00	0.11	0.07	0.10	0.11	0.12	0.25	0.37	0.44	0.52	0.46	0.05	0.07	0.03	0.06
CaO	0.01	0.02	0.00	0.02	0.03	0.00	0.40	0.67	0.47	0.73	0.49	22.38	22.57	20.10	20.95	21.01	0.01	0.00	0.00	0.00
FeO	9.73	9.50	9.85	10.01	9.62	9.85	6.29	6.15	6.36	6.55	6.26	2.43	2.21	2.17	2.36	2.14	12.66	15.88	12.64	12.64
NiO	0.36	0.34	0.40	0.36	0.38	0.37	0.09	0.09	0.11	0.05	0.08	0.04	0.05	0.06	0.04	0.06	0.33	0.22	0.43	0.40
V_2O_3	0.00	0.00	0.00	0.03	0.02	0.01	0.03	0.04	0.03	0.05	0.01	0.06	0.06	0.03	0.05	0.05	0.03	0.10	0.11	0.07
Cr_2O_3	0.05	0.01	0.01	0.04	0.00	0.02	0.41	0.45	0.48	0.39	0.37	0.93	0.74	0.90	0.79	0.75	14.24	18.92	9.83	9.85
ZnO	0.00	0.00	0.03	0.01	0.03	0.01	0.03	0.00	0.04	0.04	0.06	0.03	0.01	0.04	0.00	0.01	0.14	0.26	0.20	0.19
Total	100.01	99.84	99.98	100.28	99.85	100.01	100.12	99.71	100.00	100.15	99.93	99.81	99.53	98.69	99.81	100.25	101.04	98.80	99.93	100.07
Mg#	0.90	0.90	0.90	0.90	0.90	0.90	0.90	0.90	0.90	0.90	0.90	0.92	0.93	0.92	0.92	0.93	0.77	0.69	0.78	0.79
Cr#																	0.15	0.21	0.10	0.10

Table 2. Representative electron microprobe analyses of individual phases in the polyphase sulphide assemblages

Phase	Awaruite	Cu, Fe, Ni alloy	Pentlandite	Awaruite	Magnetite				Pentlandite		Cu, Fe, Ni alloy	Pentlandite	
Sample no.	1d-8	1d-8	1d-8	1d-8	1d-8	1d-8	2b-9	2b-9	2b-9	2b-9	6a-8	6a-8	6a-8
Spot no.	1	6	12	8	13	20	24	25	27	29	52	53	46
Concentration (wt%)													
S	0.01	0.12	33.53	0.01	0.10	0.01	0.04	0.03	32.93	33.15	0.17	26.49	30.22
Zn	0.00	0.14	0.00	0.00	0.00	0.02	0.01	0.01	0.00	0.00	0.00	0.08	0.00
Co	0.71	0.07	0.41	0.42	0.12	0.11	0.13	0.10	2.04	0.60	0.16	2.37	0.85
Ni	70.79	3.70	28.47	71.04	2.84	0.03	0.28	0.03	24.99	24.91	3.39	20.96	24.47
Fe	27.43	9.53	36.98	26.33	62.55	65.45	64.21	63.26	38.98	39.85	2.93	42.88	39.86
Cu	0.00	84.04	0.00	0.00	0.00	0.02	0.00	0.01	0.00	0.00	88.04	0.00	0.44
Total	98.93	97.59	99.39	97.79	65.60	65.65	64.68	63.44	98.94	98.51	94.68	92.77	95.84

Orthopyroxene grains were magnesian (En$_{88.4-89.5}$) with an Mg# of 0.90, exhibited high Al$_2$O$_3$ contents (3.74–5.29 wt%), low Cr$_2$O$_3$ contents (0.33–0.48 wt%), low Na$_2$O contents (≤0.11 wt%), and CaO and TiO$_2$ within the ranges 0.40–0.73 wt% and 0.05–0.18 wt% respectively. Examination of Al$_2$O$_3$ content versus Mg# (Figure 3 c) shows that the studied orthopyroxene grains are characteristic of abyssal peridotites.

Clinopyroxene was found to be augite and had a CaO content that ranged from 20.1 to 22.57 wt%. Al$_2$O$_3$ content varied from 5.85 to 7.35 wt%, and all grains had a consistent Mg# of 0.92. Cr$_2$O$_3$ content ranged from 0.69 to 0.90 wt%, Na$_2$O content from 1.14 to 1.97 wt%, and TiO$_2$ content from 0.44 to 0.52 wt%. A Cr$_2$O$_3$ content versus Mg# plot for all analysed clinopyroxene grains also shows that the samples studied are abyssal peridotite.

Spinels from the studied samples exhibited Cr# ranging from 0.10 to 0.15, and Mg# between 0.76 and 0.79. TiO$_2$ content was 0.03–0.15 wt%, MnO content was 0.10–0.14 wt%, and NiO content was 0.22–0.43 wt%. The measured MgO contents were in the range 16.36–20.16 wt%, Cr$_2$O$_3$ content varied from 9.67 to 18.92 wt%, and FeO content ranged from 12.64 to 15.88 wt%. A plot of Cr# versus Mg# also indicated that the samples studied were characteristic of abyssal peridotite.

Equilibrium pressure and temperature conditions under which the ultramafic rock formed provide information about the nature of evolution of the ophiolite mantle sequence. A single-clinopyroxene geobarometer[5] was used to calculate an equilibrium pressure, which showed a narrow range of 23–24 kbar, close to the garnet-lherzolite stability field. Two-pyroxene thermometry[6] was used to calculate an equilibrium temperature within the range 1080–1240°C. Oxygen fugacity (fO$_2$) is also important to understand mantle processes, and was calculated in this study using the calibration of Ballhaus et al.[7]. The samples studied were found to have crystallized at 0.303–0.580 log units above the FMQ buffer. Together, these pressure, temperature and oxygen fugacity equilibrium conditions suggest that these units equilibrated in the upper mantle.

Peridotites associated with oceanic crust provide important information on the processes of melt generation, fluid-phase enrichment, and mantle–melt interactions subsequent to melt extraction[8–10]. We have used the Cr# of spinel from peridotites to calculate that the samples experienced low degrees of partial melting (1–5%)[11].

The above-described samples were further studied to investigate their sulphide mineral contents. Sulphides were often concentrated in the vicinity of large orthopyroxene crystals, with pentlandite present along orthopyroxene cleavages and (occasionally) fractures (Figure 2 d). Pentlandite also occurred as irregular shaped discrete and disseminated grains and grain aggregates ranging from a few microns to millimetres in size, also in association with orthopyroxene. Composition of the pentlandite is given in Table 2. Ni content ranged between 24.91 and 28.47 wt%, Co content ranged between 0.41 and 2.04 wt%, and Cu and Zn were undetected.

Secondary Cu–Fe–Ni metal alloys occurred as rims or located along cleavages and fractures of primary sulphides. Awaruite, a Cu-rich metal alloy, and magnetite were observed to be present as secondary phases. Magnetite occurred as narrow filaments, irregular patches either within or along the border of sulphide phases, and sometimes as hosts to awaruite grains (Figure 2 f). The compositions of these phases are presented in Table 2. Awaruite contained ~71 wt% Ni and 26–27 wt% Fe. The Cu-rich metal alloy contained 84–88 wt% Cu, variable Fe (2.93–9.53 wt%), and minor Ni (3.38–3.70 wt%). A low analysis total is attributed to the presence of other elements that were not analysed. Magnetite contained an Fe content of 62.55–65.45 wt%, alongside small amounts of Ni (<0.29 wt%) and Co (~0.1 wt%).

Sulphide phases in peridotites are suggested to originate from immiscible sulphide melts that become trapped during partial melting events in the mantle residues[12]. It has been experimentally shown that the sulphide and silicate liquids are immiscible near 1100°C in the FeS–FeO–Fe$_3$O$_4$–SiO$_2$ system[13]. Partial melting of mantle materials that contains ~200–300 ppm sulphur – a commonly accepted value for the subcontinental mantle[14] – would yield a primary silicate melt and an immiscible sulphide melt if the degree of melting (mass fraction) was less than ~25% (ref. 14). As noted above, the studied Indo-Myanmar ophiolite peridotite samples experienced <5% partial melting. An 'immiscible sulphide melt' may have therefore segregated and settled to the bottom of the melting zone as a result of its higher density. This may have subsequently been incorporated into residual mantle rocks, with pentlandite in the studied samples having likely crystallized from it during cooling.

In general, dihydrogen (H$_{2,aq}$) is released during hydrothermal alteration/serpentinization of ultramafic rocks due to the oxidation of Fe^{2+} in primary silicates (via addition of water), producing Fe^{3+} in secondary minerals (e.g. magnetite commonly forms during serpentinization)[15]. A high degree of serpentization would thus evolve a significant amount of H$_{2,aq}$, and metamorphic conditions would become reducing. Awaruite is able to form in these conditions under an extremely low oxygen fugacity, a low sulphur fugacity, and a temperature exceeding 300°C (ref. 16).

It is commonly believed that pentlandite in ultramafic rocks can desulphurize to form a pure Fe–Ni bearing phase, awaruite and magnetite. This desulphurization process is triggered by the release of H$_{2,aq}$ during serpentinization. At higher oxygen and sulphur fugacities that may occur due to more intense serpentinization/steatization, awaruite breaks down to millerite and magnetite instead[15]. Experimental study shows that the development of pentlandite + awaruite + magnetite assemblages imply

hydrogen concentrations close to (or at) the solubility of dihydrogen in water: between 200°C and 300°C (ref. 15).

In conclusion, we interpret that the studied ultramafic rocks equilibrated in upper mantle at a temperature of 1080–1240°C, a pressure of 23–24 kbar and a $f\mathrm{O_2}$ between 0.303 and 0.580 log units above the FMQ buffer. Mineral compositions consistently show that the samples studied are abyssal peridotites that have undergone low degrees of partial melting, with estimated proportions ranging from 1% to 5%. The primary sulphide phase, pentlandite, could have formed by liquid immiscibility during partial melting of the mantle component of the ophiolite. Secondary metallic alloys and magnetite were produced during the serpentization process.

1. Uysal, İ., Karl, O., Delek, Y., Sadiklar, M. B., Ottley, C. J., Tiepolo, M. and Meisel, T., Coexistence of abyssal and ultra-depleted SSZ type mantle peridotites in a Neo-Tethyan Ophiolite in SW Turkey: Constraints from mineral composition, whole-rock geochemistry (major–trace–REE–PGE), and Re–Os isotope systematics. *Lithos*, 2012, **132–133**, 50–69.

2. Singh, A. K., Devi, L. D., Singh, N. I., Subramanyam, K. S. V., Singh, R. K. B. and Satyanarayanan, M., Platinum-group elements and gold distributions in peridotites and associated podiform chromitites of the Manipur Ophiolitic Complex, Indo-Myanmar Orogenic Belt, Northeast India. *Chem. Erde-Geochem.*, 2012, **73**, 117–145.

3. Ningthoujam, P. S., Dubey, C. S., Guillot, S., Fagion, A.-S. and Shukla, D. P., Origin and serpentinization of ultramafic rocks of Manipur Ophiolite Complex in the Indo-Myanmar subduction zone, Northeast India. *J. Asian Earth Sci.*, 2012, **50**, 128–140.

4. Singh, A. K., Petrology and geochemistry of abyssal peridotites from the Manipur ophiolite complex, Indo-Myanmar orogenic belt, Northeast India: implication for melt generation in mid-oceanic ridge environment. *J. Asian Earth Sci.*, 2013, **66**, 258–276.

5. Nimis, P. and Taylor, W. R., Single clinopyroxene thermobarometry for garnet peridotites Part–I. Calibration and testing of a Cr-in-Cpx barometry and an enstatite-in-Cpx thermometer. *Contrib. Mineral. Petrol.*, 2000, **139**, 541–554.

6. Nickel, K. G., Brey, G. P. and Kogarko, L., Orthopyroxene-clinopyroxene equilibria in the system CaO–MgO–Al$_2$O$_3$–SiO$_2$ (CMAS): new experimental results and implications for two-pyroxene thermometry. *Contrib. Mineral. Petrol.*, 1985, **91**, 44–53.

7. Ballhaus, C., Berry, R. F. and Green, D. H., Oxygen fugacity control in the Earth's upper mantle. *Nature*, 1990, **348**, 437–440.

8. Johnson, K. T. M., Dick, H. J. B. and Shimizu, N., Melting in the oceanic upper mantle; anion microprobe study of diopsides in abyssal peridotites. *J. Geophys. Res.*, 1990, **95**, 2661–2678.

9. Seyler, M., Toplis, M. J., Lorand, J. P., Luguet, A. and Cannat, M., Clinopyroxene microtextures reveal incompletely extracted melt in abyssal peridotites. *Geology*, 2001, **29**, 155–158.

10. Dick, H. J. B. and Bullen, T., Chromian spinal as a petrogenetic indicator in abyssal and alpine-type peridotites and spatially associated lavas. *Contrib. Miner. Petrol.*, 1984, **86**, 54–76.

11. Hellebrand, E., Snow, J. E., Hoppe, P. and Hofmann, A. W., Garnet field melting and late stage refertilization in residual abyssal peridotites from the Central Indian ridge. *J. Petrol.*, 2002, **43**, 2305–2338.

12. Frick, C., The sulphides in griquaite and garnet–peridotite xenoliths in kimberlite. *Contrib. Mineral. Petrol.*, 1973, **39**, 1–16.

13. MacLean, W. H., Liquidus phase relations in the FeS–FeO–Fe$_3$O$_4$–SiO$_2$ systems and their applications in geology. *Econ. Geol.*, 1969, **64**, 865–884.

14. Keays, R. R., The role of komatiitic and picritic magmatism and S-saturation in the formation of ore deposits. *Lithos*, 1995, **34**, 1–18.

15. Klein, F. and Bach, W., Fe–Ni–Co–O–S phase relations in peridotite – seawater interactions. *J. Petrol.*, 2009, **50**(1), 37–59.

16. Frost, B. R., On the stability of sulfides, oxides and native metals in serpentinite. *J. Petrol.*, 1985, **26**, 31–63.

17. Takahashi, E., Uto, K. and Schilling, J. G., Primary magma compositions an Mg/Fe ratios of their mantle residues along Mid-Atlantic Ridge 29 N to 73 N. *Tech. Rep. Inst. Study Earth's Inter. Okayama Univ. Ser. A*, 1987, **9**, 1–14.

18. Khedr, M. Z. and Arai, S., Origin of Neoproterozoic ophiolitic peridotites in south Eastern Desert, Egypt, constrained from primary mantle mineral chemistry. *Miner. Petrol.*, 2013, **107**, 807–828.

19. Ishii, T., Robinson, P. T., Maekawa, H. and Fiske, M., Petrological studies from diapric serpentinite seamounts in the Izu Ogazawara Mariana forarc, Leg 125. In *Proceedings of the Ocean Drilling Program, Scientific Result* (eds Fryer, P., Pearce, J. A. and Stokking, L. B.), Ocean Drilling Program, College Station, Texas, USA, 1992, pp. 445–485.

20. Seo, J., Oh, C. W., Choi, S. G. and Rajesh, V. J., Two ultramafic rock types in the Hongseong area, South Korea: Tectonic significance for northeast Asia. *Lithos*, 2013, **175–176**, 30–39.

21. Constantin, M., Gabbroic intrusions and magmatic metasomatism in harzburgites from the Garrett transform fault: implications for the nature of the mantle–crust transition at fast spreading ridges. *Contrib. Mineral. Petrol.*, 1999, **136**, 111–130.